Published in final edited form as:
J Mol Biol. 2008 February 22; 376(3): 827–838.

Role of Intrinsic Flexibility in Signal Transduction Mediated by the Cell Cycle Regulator, p27^{Kip1}

Charles A. Galea[1], **Amanda Nourse**[2], **Yuefeng Wang**[1], **Sivashankar G. Sivakolundu**[1], **William T. Heller**[3], and **Richard W. Kriwacki**[1,4,*]

1 *Department of Structural Biology, St. Jude Children's Research Hospital, 332 North Lauderdale St., Memphis, Tennessee 38105, USA*

2 *Hartwell Center for Bioinformatics and Biotechnology, St. Jude Children's Research Hospital, 332 North Lauderdale St., Memphis, Tennessee 38105, USA*

3 *Center for Structural Molecular Biology and Chemical Sciences Division, Oak Ridge National Laboratory, Oak Ridge, Tennessee 37831*

4 *Department of Molecular Sciences, University of Tennessee Health Sciences Center, Memphis, TN, USA*

Summary

p27^{Kip1} (p27), which controls eukaryotic cell division through interactions with cyclin-dependent kinases (Cdks), integrates and transduces pro-mitogenic signals from various non-receptor tyrosine kinases (NRTKs) by orchestrating its own phosphorylation, ubiquitination and degradation. Intrinsic flexibility allows p27 to act as a "conduit" for sequential signaling mediated by tyrosine and threonine phosphorylation and ubiquitination. While the structural features of the Cdk/cyclin-binding domain of p27 are understood, how the C-terminal regulatory domain coordinates multi-step signaling leading to p27 degradation is poorly understood. We show that the 100-residue p27 C-terminal domain is extended and flexible when p27 is bound to Cdk2/cyclin A. We propose that the intrinsic flexibility of p27 provides a molecular basis for the sequential signal transduction conduit that regulates p27 degradation and cell division. Other intrinsically unstructured proteins possessing multiple sites of post-translational modification may participate in similar signaling conduits.

Keywords

cell cycle; cyclin-dependent kinase inhibitor; disordered protein; intrinsically unstructured protein; p27^{Kip1}

Introduction

The cyclin-dependent kinase inhibitor (CKI) p27^{Kip1} [1,2,3] is a small intrinsically unstructured protein (IUP)[4] that regulates cell proliferation through interactions with cyclin-dependent kinases (Cdks).[5] For example, in G_1 phase, an initially high level of p27 blocks progression from G_1 to S phase of the cell division cycle by inhibiting Cdk2/cyclin A and Cdk2/cyclin E.[6,7] The level of p27, which is controlled by translational regulation[8] and ubiquitination-

*To whom correspondence should be addressed: Dr. Richard Kriwacki, Department of Structural Biology, St. Jude Children's Research Hospital, 332 North Lauderdale St., Memphis, TN USA 38105. Tel.: +1 901 495-3290. Fax: +1 901 495-3032. E-mail: richard.kriwacki@stjude.org (R.W. Kriwacki).

dependent proteolysis,[8,9] must drop for Cdk2 complexes to be fully activated and for cell division to progress. Ubiquitination of p27 at the G_1/S transition is regulated by a two-step mechanism that involves phosphorylation of p27, first on tyrosine 88 (Y88) by one of several non-receptor tyrosine kinases (NRTKs) and second on threonine 187 (T187) by Cdk2.[10]

Enhanced ubiquitination-mediated degradation of p27 [11] is common in human tumors[12] and is associated with poor clinical prognosis.[13] p27 is ubiquitinated through at least two pathways: 1) free, unphosphorylated p27 is ubiquitinated by KPC1[14,15] and 2) p27 bound to Cdk2/cyclin complexes is ubiquitinated by SCF/Skp2.[12,16] Up-regulation of the two-step p27 phosphorylation mechanism by the oncogenic NRTKs, Bcr-Abl and Src,[10,17] was recently shown to promote SCF/Skp2-mediated p27 loss in chronic myelogenous leukemia (CML)[10] and breast cancer cells,[17] respectively. While the general features of the two-step phosphorylation mechanism are understood, the full extent to which the unusual structural features of p27—an intrinsically unstructured protein[4]—contribute to the mechanism is poorly understood.

The intrinsic flexibility of p27 allows its interactions with Cdk2/cyclin A and SCF/Skp2 to be modulated by phosphorylation of tyrosine and threonine residues at opposite ends of the p27 polypeptide chain. Prior to phosphorylation, Y88, which is found at the C-terminal end of the so called “kinase inhibitory domain” (KID) of p27 that binds and inhibits Cdk2 (Fig. 1a), is lodged in the ATP binding pocket of Cdk2 thereby inhibiting catalysis by blocking access to ATP. However, due to putative dynamics involving the 3_{10} helix containing Y88 fluctuating into and out of the ATP binding pocket,[18] Y88 within p27/Cdk2/cyclin A complexes is accessible for phosphorylation by NRTKs.[10] Following phosphorylation — step 1 of the two-step mechanism —Y88 and the entire 3_{10} helical segment of the KID are ejected from the ATP binding pocket of Cdk2. While p27 remains bound to Cdk2/cyclin A, ejection of phosphorylated Y88 and the 3_{10} helix restores significant catalytic activity, allowing Cdk2 to phosphorylate T187 within the C-terminus of the same p27 molecule that is bound to Cdk2—step 2 of the two-step mechanism. The uni-molecular nature of step 2 [10] requires that the C-terminus of p27 “folds back” to allow T187 to be phosphorylated by Cdk2. While much is known about the structural and dynamic features of the KID of p27 both in the free state[4,19] and when bound to Cdk2/cyclin A,[18] detailed information on these properties for the C-terminal region of p27 is not available. Herein we report results from a number of techniques that fully describe the structural features of full-length p27 and explain how T187 can be phosphorylated by Cdk2 via the pseudo uni-molecular mechanism. These results highlight the importance of the intrinsic flexibility of p27 in mediating the multi-step signal transduction pathway which controls cell division in eukaryotes.

Results

NMR Studies of the C-terminus of p27 in the p27/Cdk2/cyclin A ternary complex

p27 is comprised of an N-terminal domain (p27-KID, residues 22–104) that binds and inhibits Cdk/cyclin complexes and a C-terminal domain (residues 105–198, p27-C) that contains several sites of post-translational modification, including T187 (Fig. 1a). While the structure of p27-KID in the free state[4,20] and bound to Cdk2/cyclin A[10,18] have been characterized in detail, little information is available on the structure of p27-C and how this domain orchestrates the two-step phosphorylation mechanism. We probed the structure and dynamics of the p27 C-terminus using NMR spectroscopy, first by studying the isolated C-terminal domain (p27-C) and second by studying isotope-labeled p27 bound to Cdk2/cyclin A. The 2D ^{1}H-^{15}N HSQC spectrum of ^{15}N-labeled p27-C (Fig. 1b, green) exhibited the limited chemical shift dispersion that is typical of intrinsically unstructured proteins (IUPs). Further, secondary $^{13}C_{\alpha}$ chemical shift values ($\Delta\delta$ $^{13}C_{\alpha}$) (Supplementary Fig. 1a) did not indicate the existence of highly populated secondary structure and {^{1}H}-^{15}N heteronuclear (hetNOE) values (Supplementary

Fig. 1b) were almost exclusively negative, consistent with frequent, random amide group fluctuations on the high ps-low ns time scale. In addition, the chemical shift values of most amides within p27-C were very similar for the isolated domain and this domain in the context of $^{2}H/^{15}N$-p27 bound to Cdk2/cyclin A (Fig. 1b, red). The structural independence of p27-C was confirmed by showing that resonances for p27-KID bound to Cdk2/cyclin A (Fig. 1c, blue) were recapitulated in the 2D ^{1}H-^{15}N TROSY spectrum of $^{2}H/^{15}N$-p27/Cdk2/cyclin A (Fig. 1c, red). Together, these results indicated that p27-C in the p27/Cdk2/cyclin A complex is an independent, flexible domain that lacks secondary structure. These NMR results provide detailed insights into the average conformation and dynamics for most residues of p27-C within the biologically active p27/Cdk2/cyclin A complex. However, chemical shift and hetNOE values reflect only the local environment of nuclei within the polypeptide backbone and do not define the global structure of this domain.

Molecular dynamics computations

Based on our knowledge from NMR that p27-C is an independent, intrinsically unstructured domain, we used molecular dynamics (MD) computations to better understand the overall structure and dynamics of p27-C in the context of the p27/Cdk2/cyclin A complex. During the 12.7 ns MD computation, residues of p27 were only under the influence of the Amber force field. This allowed residues within p27-C to explore energetically allowed conformations constrained only by local, intra-p27 interactions and longer-range, intermolecular interactions with Cdk2/cyclin A. The use of a continuum model of water, rather than explicit water, allowed efficient sampling of conformational space for this rather large molecular system during the ~13 ns trajectory. Interestingly, the segment of p27-C immediately following the KID protruded at an abrupt angle perpendicular to the surface of Cdk2/cyclin A and exhibited limited flexibility (Fig. 2a). The phi and psi torsion angles for residues in this region (residues 110–140) explored a more limited range of values than did those closer to the C-terminus (Fig. 2b). The abrupt protrusion of p27-C from the surface of the p27-KID/Cdk2/cyclin A complex may arise due to electrostatic repulsion of acidic amino acids in p27-C between residues 110–140 and the largely negatively charged surface of p27-KID/Cdk2/cyclin A proximal to the point of protrusion (Fig. 2c, d). This electrostatic guiding may cause the more distal segment of p27-C (residues 150–198) to assume highly extended conformations. These features give rise to large values of the end-to-end distance for complexes within the entire p27/Cdk2/cyclin A ensemble (average end-to-end distance, 138 ± 9 Å; Supplementary Fig. 2). Based on the general absence of stable secondary structure within p27-C throughout the MD trajectory, we conclude that the conformational properties of residues within p27-C in the ensemble of MD structures are consistent with the NMR findings for this segment.

Hydrodymanic analysis of p27/Cdk2/cyclin A

We used two techniques, analytical ultracentrifugation (AUC) and small-angle X-ray scattering (SAXS), to study the size and shape of the p27/Cdk2/cyclin A ternary complex and related findings from these two techniques to those from MD computations and NMR spectroscopy.

AUC studies—Analysis of AUC data showed that p27/Cdk2/cyclin A sedimented as a mono-disperse 1:1:1 species with an *s*-value of 3.98 S, a $(f/f_0)_w$ (weight-average frictional ratio, f/f_0) value of 1.63 and a molar mass of 87,603 Da, close to its theoretical molar mass of 86,796 Da (Fig. 3a). The $(f/f_0)_w$-value reflects significant extension of p27-C from the globular core of the p27/Cdk2/cyclin A complex. The mono-disperse nature of the ternary complex was confirmed by sedimentation equilibrium analysis, which showed a single species of mass 86,761 Da (Supplementary Fig. 3). We compared the experimental *s*-value with those calculated from explicit molecular structures of p27/Cdk2/cyclin A taken at 100 ps intervals from the equilibrated portion of the MD trajectory. To compare the experimental and theoretical values, the experimental value was converted to standard conditions (water solution at 20 °C),

giving an $s_{20,w}$-value of 4.28 S. Theoretical $s_{20,w}$-values for p27/Cdk2/cyclin A were calculated using structures from the MD calculations with the program HYDROPRO21,22 (Fig. 3b). The average $s_{20,w}$-value thus obtained was 4.24 ± 0.07 S. While the theoretical $s_{20,w}$-values reflected significant structural fluctuations, ranging from 4.05 S to 4.35 S, the agreement observed between the average of these values, 4.24 ± 0.07 S, and the experimental $s_{20,w}$-value, 4.28 S, indicated that the molecular structures comprising the MD ensemble accurately represented the actual molecular ensemble as regards to their hydrodynamic properties based on AUC measurements. In addition, while p27/Cdk2/cyclin A sediments with a narrow distribution of *s*-values, calculating the two-dimensional *c* (*s*,f/f_0) distribution in the program SEDFIT (www.analyticalultracentrifugation.com) revealed that the peak at 4.00 S was best fit using a distribution of f/f_0-values (Fig. 3c). This finding strongly suggests that conformational fluctuations of p27-C within the ternary complex give rise to a distribution of molecular shapes, further strengthening the view that the ensemble of MD structures accurately represents conformational features of p27/Cdk2/cyclin A.

SAXS studies—The reduced SAXS intensity profile for p27/Cdk2/cyclin A (Fig. 4a & b) was analyzed to provide additional insights into the structure of the ternary complex, especially with regard to the conformation of p27-C. The data, which were collected at a concentration of 5 mg/mL, displayed evidence of slight aggregation at low *q*, which had limited impact on the data past $q = 0.025$ Å^{-1}. Data collected at 2 mg/mL (not shown) were consistent with the data collected at 5 mg/mL, which indicates a lack of concentration-dependent effects. Performing a fit over the range $q = 0.025$ Å^{-1} to 0.040 Å^{-1}, resulted in an R_g value of 40.6 ± 4.8 Å. While this *q*-range is beyond the normally applicable Guinier region,23 the data was well-fit. The forward scatter was 0.332/cm, which is ~15% above the value expected based on the concentration and molecular weight of the complex and indicates that most of the sample consists of monomers. Analysis of the data over the range $q = 0.025$ Å^{-1} to 0.070 Å^{-1} according to Debye[24] which treats the particle as an unfolded, Gaussian coil, yielded an R_g of 38.5 ± 8.2 Å. The distance distribution function *P* (*r*) was derived by fitting *q*-values from 0.025 Å^{-1} to 0.15 Å^{-1} (Fig. 4c). The value for the maximal diameter of the molecule (d_{max}) was 130 ± 10 Å. The R_g determined from the *P* (*r*) fitting was 40.2 ± 4.8 Å. This value is in good agreement with both the Guinier- and Debye- derived values and provides confidence that the results of the analyses are reasonable. The *P* (*r*) curve suggests a somewhat extended particle.

Intensity profiles calculated from explicit molecular structures of p27/Cdk2/cyclin A from the MD trajectory were calculated using the program ORNL_SAS[25] and then compared with experimental data over the range $q = 0.025$ Å^{-1} to 0.20 Å^{-1} (Fig. 4a). The contribution of p27-C within the p27/Cdk2/cyclin A ternary complex was assessed by comparing fits of the intensity profiles computed using p27-KID/Cdk2/cyclin A,[18] which lacks p27-C, and using p27/Cdk2/cyclin A, in which p27-C was manipulated to be highly extended (p27^{EX}), with the experimental intensity profile (Fig. 4a). The χ^2 values for these two fits were 0.595 and 0.590, respectively. The calculated intensity profiles suggest that the p27^{EX} bound to Cdk2/cyclin A contributed little to the model intensity profile over this *q*-range. Importantly, the intensity profile calculated using the ensemble of p27/Cdk2/cyclin A structures generated by MD fitted the experimental data much better than did those calculated using the two individual ternary complex structures ($\chi^2 = 0.298$). The improved fit to experimental data was most apparent for *q*-values from 0.05 Å^{-1} to 0.10 Å^{-1}, where the data and ensemble profile had a flattened character compared to the other two computed intensity profiles that is more consistent with the shape of the data (Fig. 4b). The apparent shift of the other two profiles results from the scaling used to compare the model intensity profiles to the data by ORNL_SAS, which minimizes the χ^2 value through the use of a scaling constant and a baseline shift. If the model profiles were made to be more consistent in this range, then other portions of the curve would be fit less well, resulting in a higher χ^2 value. Further, the inherent slope of the model profiles of the truncated complex and the p27^{EX} complex in that particular region would remain less

true to the character of the data than the intensity profile from the ensemble of structures. This *q*-range corresponds to distances ranging from ~60 Å to ~120 Å that are impacted to a lesser degree by the slight aggregation observed than the lower *q*-values, such as those used for the Guiner fitting.[23] These distances are also likely to be most impacted by the ensemble of p27 conformations that are significantly more compact than the $p27^{EX}$, which will only contribute slightly to the intensity profile in this range due to the much greater length of the structure. Beyond 0.10 $Å^{-1}$, the p27-C in the ensemble also produces additional interatomic distances <60 Å that are not present in the other two structures, resulting in the differences between the model intensity profiles. The R_g values determined from the second moments of the model *P (r)* curves calculated for the truncated structure, the $p27^{EX}$ structure and the ensemble of structures were 25.5 Å, 61.4 Å and 32.8 Å, respectively. Taken together, the SAXS results suggest that the ensemble of MD structures is a better representation of the structure of p27/Cdk2/cyclin A in solution than is the individual structure containing $p27^{EX}$, but that the actual ensemble in solution may contain states that are more extended than the structures sampled by MD.

The low-resolution consensus envelope model was generated from the SAXS intensity profile data using the program GA_STRUCT[26] (Fig. 4d). The globular portion of the p27/Cdk2/cyclin A complex (~80 Å long, ~60 Å wide) could readily be accommodated within one end of the computed elongated envelope (~175 Å long, ~60 Å wide), while the extended conformations of the p27 C-terminus for structures generated during the MD simulation could be accommodated within the remaining volume of this envelope (Fig. 4d). It is important to note that the computed molecular envelope is of uniform density and, therefore, the structural agreement between this model and the ensemble of molecular structures generated from the MD simulations must be interpreted qualitatively.[27] However, the general dimensions and elongated nature of the computed molecular envelope are in good agreement with the general shape of the superposed molecular structures (Fig. 4d). Because the computed molecular envelope is of uniform density, it is not possible to differentiate between ordered and disordered regions of the complex based on the results of the modeling.

Discussion

The results of our study provide the first detailed insights into the conformation of full-length p27 when bound to Cdk2/cyclin A, the form of p27 that blocks eukaryotic cell division by inhibiting the catalytic activity of this and several other Cdk/cyclin complexes. The crystal structure of p27-KID bound to Cdk2/cyclin A determined by x-ray diffraction[18] provided the first insights into how p27 binds and inhibits Cdks. More recently, NMR spectroscopy studies have provided detailed insights into how the Cdk2/cyclin A-bound conformation of p27-KID is altered by phosphorylation of Y88.[10] These studies showed that the C-terminus of p27 does not interact extensively with the Cdk/cyclin complex, even though it plays an important role in the regulation of p27-mediated cell cycle arrest. We and others have previously reported that CD spectropolarimetry analysis showed that full-length p27 is intrinsically unstructured.[4,28] While the N-terminal KID of free p27 contained regions of transient structure, the C-terminal domain (p27-C, residues 105–198) lacked detectable secondary structure. In addition, analysis by NMR spectroscopy showed that, in the absence of its Cdk/cyclin binding partners, the N- and C-termini of p27 do not interact.[4] However, these studies did not provide a detailed understanding of the structure of p27-C either in isolation or when the KID of full-length p27 is bound to the Cdk/cyclin complex.

In the present study, we have used a variety of techniques to gain a comprehensive understanding of the structure of p27-C. First, we studied average secondary structure and ps-ns time scale dynamics of individual residues of p27-C using NMR spectroscopy. $\Delta\delta\ ^{13}C_{\alpha}$ values for residues of p27-C indicated a general lack of secondary structure, while most

backbone amide moieties exhibited negative hetNOE values, demonstrating that long-range interactions between different regions within p27-C do not occur.

Second, based on our past experience using unrestrained MD computations to explore the inherent conformational properties of p27-KID,[20] we used MD to explore the conformational features of p27-C when p27 was bound to Cdk2/cyclin A. Surprisingly, p27-C remained quite highly extended during the trajectory, rather than assuming more compact conformations as might be expected. Analysis of phi and psi torsion angles showed that conformational freedom was limited for residues in p27-C that were close to the surface of Cdk2/cyclin A, and that RMSD values for these torsion angles increased toward the extreme C-terminus furthest away from Cdk2/cyclin A. Visual inspection of the p27/Cdk2/cyclin A complex indicated that this restricted motion may be due to electrostatic repulsion between the molecular surface of Cdk2/cyclin A and p27-C which "steers" the p27 polypeptide backbone away from the globular core of Cdk2/cyclin A. Finally, torsion angles and RMSD values observed for p27-C during the MD trajectory were consistent with $\Delta\delta\ ^{13}C_{\alpha}$ values determined by NMR spectroscopy. The overall general agreement of results obtained by NMR spectroscopy and MD, regarding the conformation of p27-C, allowed us to use evenly sampled molecular structures from the MD trajectory to represent the solution conformation of full-length p27/Cdk2/cyclin A.

The third approach employed to characterize the conformation of p27-C was to use AUC and SAXS to analyze the hydrodynamic properties of the p27/Cdk2/cyclin A complex. These techniques allowed direct measurement of hydrodynamic properties that reflect the average, global conformation of this protein complex in solution, in contrast to the local nature of chemical shift and hetNOE values determined by NMR spectroscopy. We showed that molecular structures obtained during the MD trajectory, in which p27-C is highly extended, were consistent with both AUC sedimentation velocity and SAXS data by calculating *s*-values (AUC) and intensity profiles (SAXS) using an ensemble of MD-generated molecular structures. The agreement between computed and experimentally determined values from AUC and SAXS strongly suggested that the MD structures are a true representation of the solution structure of p27/Cdk/cyclin A and the extent to which the p27-C portion of this complex samples conformational space.

Two types of post-translational modification, phosphorylation and ubiquitination, regulate the Cdk inhibitory activity and degradation of p27 in eukaryotic cells. These modifications occur in sequential order, and include a two-step phosphorylation mechanism followed by ubiquitination. The first step involves phosphorylation of Y88 by NRTKs and partial "re-activation" of Cdk2 within the p27/Cdk2/cyclin A complex[10]. In the second step, re-activated Cdk2 phosphorylates T187 located toward the C-terminus of the 100-residue long C-terminal domain of p27. Subsequently, phosphorylated T187 and several neighboring residues are recognized by the SCF/Skp2 E3 ubiquitin ligase and p27 is poly-ubiquitinated at currently unknown sites. This modification cascade finally leads to the elimination of p27 through 26S proteasome-mediated degradation and, consequently, de-repression of the major blockade to progression of the cell division cycle from G_1 to S phase. Although the degradation mechanism described above applies specifically to the interaction of p27 with Cdk2/cyclin A, p27 binds to many different Cdk/cyclin targets *in vivo* and it is likely that this multi-step modification cascade regulates p27 within its complex with Cdk2/cyclin E and possibly within complexes comprising Cdk1 and either cyclin A or cyclin E.

Here we have shown that the C-terminal domain of p27 adopts a disordered and quite highly extended conformation when p27 is bound to Cdk2/cyclin A. The p27 C-terminus functions as a regulatory domain that is structurally independent of the N-terminal domain, which itself binds tightly and specifically to several different Cdk/cyclin complexes involved in regulating the G_1/S cell cycle transition. The C-terminal domain acts as a flexible "conduit" for signal

transduction, which detects a specific signal from NRTKs (phosphotyrosine 88) and, through the catalytic activity of Cdk2, mediates conversion of this signal into a second signal, phospho-threonine 187 (pT187). The phospho-threonine 187 signal, in turn, is functionally transduced through poly-ubiquitination (of p27) by SCF/Skp2 in a pT187-dependent manner which signals the 26S proteasomal degradation of p27. While not sampled in our brief MD trajectory, our previous biochemical data[10] support the view that T187 within the p27 C-terminus frequently approaches the Cdk2 active site within individual ternary complexes. The results of the structural analysis reported herein support this model by showing that p27-C lacks discreet structure and is highly flexible. While extended in the MD trajectory, p27-C appears to be sufficiently unrestrained to occasionally sample conformations in which T187 “folds back” to encounter the Cdk2 active site (Fig. 5). Based on our observation that the surface of Cdk2/cyclin A near the ATP binding site bears negative charge, we propose that electrostatic interactions between this surface and a cluster of positively charged residues at the p27 C-terminus adjacent to T187 facilitate interactions between T187 and the Cdk2 substrate binding site. If Y88 of p27 is phosphorylated when these interactions occur, then the oncogenic signal from NRTKs can be transduced through phosphorylation of T187 and subsequent ubiquitination and degradation of p27. If Y88 is not phosphorylated, no signal is transduced and Cdk2/T187 encounters are catalytically unproductive. The extended nature and flexibility of the 100 residue-long p27 C-terminus makes it possible for T187 to constantly sense the signaling status of Y88 (i.e. absence or presence of phosphorylation). In addition to flexibility within p27-C being critical for signaling along this conduit, we previously discussed the importance of Y88 being able to fluctuate between ATP binding pocket-bound and solvent-exposed conformations so that Y88 is accessible for phosphorylation by NRTKs.[10] More recently, tyrosine 88 and a second tyrosine residue of p27, tyrosine 74 (Y74), were shown to be phosphorylated by the NRTK, Src, in breast cancer cells.[17] This observation suggests that not only does the Y88-containing segment of p27 experience conformational fluctuations, but that the segment containing Y74, within the β-hairpin that is sandwiched against the N-terminal β-sheet lobe of Cdk2[18] (Fig. 1), also experiences conformational fluctuations that make its side-chain available for phosphorylation by Src. Phosphorylation of Y74 by Src may disrupt local interactions between p27 and Cdk2, which may in turn enhance the accessibility of Y88 to NRTKs and its subsequent phosphorylation. This proposal is supported by data showing that mutation of Y74 to glutamic acid disrupts interactions between p27-KID and Cdk2/cyclin A (Yuefeng Wang and Richard Kriwacki, unpublished data). Thus, this signal transduction conduit may have evolved to allow signal amplification through multiple tyrosine phosphorylation events, one at Y88 which partially re-activates Cdk2 and a second at Y74 which amplifies the initial signal. Importantly, coupling of these elements within this signal transduction conduit entirely depends on the ability of p27 to sample multiple conformations, even when bound to Cdk2/cyclin A. Finally, the flexibility and solvent accessibility of the segment of p27 containing phosphorylated T187, allow it to be readily recognized and bound by SCF/Skp2,[29] and subsequently ubiquitinated and degraded thus terminating the signaling pathway.

We conclude that the extensive flexibility of p27, which stems from its general character as an intrinsically unstructured protein, is of central importance in the multi-step phosphorylation/ubiquitination signal transduction pathway that regulates cell division. Protein flexibility has been shown to be critical in other signaling pathways. For example, the ability of the Wiskott–Aldrich syndrome protein to undergo structural rearrangements in response to allosteric signals is critical for remodeling of the actin cytoskeleton.[30] Further, substrates of kinases and phosphatases are often specifically targeted for catalysis not only through specific interactions at or near the catalytic site, but also through remote docking interactions mediated by short recognition elements;[31,32] these two types of recognition sites are often connected by intrinsically unstructured polypeptide segments.[31,32,33] p27, both a Cdk inhibitor and substrate, exhibits these latter features. p27 specifically recognizes Cdk/cyclin complexes

through interactions mediated by multiple short recognition elements connected by flexible polypeptide segments. For example, the RxLFG motif at the N-terminus of the p27 KID binds specifically to cyclin A, a second region within the KID (residues 60–82) binds specifically to the N-terminal β-sheet lobe of Cdk2, the Y88 region binds in the ATP binding pocket of Cdk2 and, finally, the region near T187 binds the substrate binding site of Cdk2. Polypeptide flexibility between the multiple recognition elements in p27, and those in many other examples,[31] affords the potential to interact with multiple targets. This concept was first proposed as the basis for the ability of $p21^{Waf1}$, a p27 homolog, to promiscuously inhibit several different Cdk/cyclin complexes that regulate cell division.[33] While previous studies established the importance of flexibility in molecular recognition by kinase substrates and inhibitors, the coupling of post-translational modifications within the multiple, flexible short recognition elements of p27 affords a level of signaling complexity that has not previously been observed. Flexible regions containing tyrosines 74 and 88 coordinate responses to signaling by NRTKs, which are integrated and transduced through partial reactivation of Cdk2, phosphorylation of T187 within the flexible C-terminus and recognition of this flexible phospho-threonine-specific recognition element by SCF/Skp2 which poly-ubiquitinates p27. The end point of this signaling conduit is recognition and degradation of poly-ubiquitinated p27 by the 26S proteasome. The lack of tertiary structure and intrinsic flexibility within p27 allows its many short recognition elements to orchestrate signaling along this conduit. We propose that many of the thousands of other eukaryotic IUPs known to play roles in signaling and regulation do so through similarly complex, multi-step signaling pathways and that the molecular events which transmit these molecular signals depend on intrinsic protein flexibility. Utilizing intrinsic protein flexibility in this way allows the transduction of multiple signals within a single protein complex due to the ability of different motifs within one polypeptide to "communicate" with each other. A challenge for the future is to identify the sequence signatures of the individual recognition elements within IUPs that comprise multi-step signaling pathways (e.g. Y88 as a target of NRTKs, T187 as a target of Cdk2, and unknown sites as targets for ubiquitination by SCF/Skp2) and to begin to decipher the complex signaling pathways that they control.

Materials and Methods

Protein preparation

Human Cdk2 (phosphorylated on T160), truncated cyclin A (residues 173–432), and full-length human p27 and fragments containing residues 22–104 (p27-KID) and 105–198 (C-terminal domain, termed p27-C) were expressed in *E. coli* and purified using established procedures.[34,35] Protein purity and identity were confirmed by SDS-PAGE and mass spectrometry. Isotope-labeled p27 ($^{2}H/^{15}N$), p27-KID ($^{2}H/^{15}N$) and p27-C ($^{13}C/^{15}N$) were prepared in MOPS-based minimal media[36] using established procedures.[10] After the individual proteins were combined, the ternary complexes, p27/Cdk2/cyclin A and p27-KID/Cdk2/cyclin A, were purified using gel filtration chromatography (Superdex 200, Amersham-Pharmacia) in 20 mM buffer (HEPES for SAXS or Tris for AUC), pH 7.5, 300 mM NaCl and 5 mM DTT.[10]

NMR spectroscopy

Samples of p27-KID/Cdk2/cyclin A and p27/Cdk2/cyclin A were exchanged into NMR buffer (20 mM potassium phosphate, pH 6.5, 50 mM arginine, 8% (v/v) $^{2}H_2O$, 5 mM DTT and 0.02% (w/v) sodium azide) and concentrated to 0.3 mM by ultrafiltration (Centricon units, Amicon). 2D ^{1}H-^{15}N HSQC spectra for p27, p27-KID and p27-C and 2D 1H-15N TROSY spectra for p27-KID/Cdk2/cyclin A and p27/Cdk2/cyclin A were recorded at 35 °C using a Bruker Avance 800 MHz spectrometer equipped with a cryogenically-cooled TCI probe. Backbone resonance assignments for $^{13}C/^{15}N$-labeled p27-C were made through the analysis of constant time (CT)-HNCA,[37] CT-HN (CO)CA,[38] CT-HNCACB[39] and CT-HN (CO)CACB[40] spectra recorded

at 25 °C in 20 mM potassium phosphate, pH 6.5, 50 mM NaCl, 8% (v/v) ^2H_2O, 5 mM DTT and 0.02% (w/v) sodium azide using a Bruker Avance 600 MHz spectrometer equipped with a cryogenically-cooled TCI probe. $\{^1H\}^{-15}N$ heteronuclear nuclear Overhauser effect (hetNOE) values were determined from 2D HSQC spectra recorded at 600 MHz with and without ^1H pre-saturation at 25 °C. Spectra were processed using NMRPipe software[41] and analyzed using Felix software (Accelerys, Inc.). For all spectra, the ^1H dimension was referenced to external TSP and the ^{13}C and ^{15}N dimensions were referenced indirectly.[42] Secondary $^{13}C_\alpha$ chemical shift values ($\Delta\delta\ ^{13}C_\alpha$) were calculated by subtracting sequence-dependent random coil values from the experimental values.[43]

Analytical ultracentrifugation (AUC)

AUC experiments were performed using a ProteomeLab XL-I analytical ultracentrifuge with an eight-hole An-50 Ti rotor (Beckman Coulter, Fullerton, CA). The partial specific volume (at 20 °C), hydration and molecular weight for the proteins based on their amino acid composition were calculated as well as the density and viscosity of the buffer (50 mM sodium phosphate pH 7.0, 150 mM NaCl, 5 mM DTT) using the computer program SEDNTERP (www.bbri.org/rasmb/rasmb.html). For the sedimentation velocity experiments the loading volume, 400 μl, was identical for the reference and sample chambers of the double-sector centrepiece. Following a 3 hour temperature equilibration at 20 °C at rest, the rotor was accelerated to 50,000 rpm and refractive index profiles were recorded in 1 min intervals with the Rayleigh interference optical system. Interference fringe displacement profiles were analysed with the software SEDFIT (www.analyticalultracentrifugation.com) using the continuous sedimentation coefficient distribution *c(s)* model and the two-dimensional size-and-shape distribution $c(s,f/f_0)$ model. The $c(s)$ distribution is based on a single weight-average frictional ratio $(f/f_0)_w$ of all the sedimenting species and the $c(s,f/f_0)$ model on the differential distribution of sedimentation coefficients and frictional ratios.[27–30] The positions of the meniscus and bottom, as well as time-invariant and radial noises, were fitted. The *s*-value of the protein was determined by integration of the main peak of *c(s)*. A two-dimensional size-shape distribution, $c(s,f/f_0)$ (*s*-distribution versus f/f_0-distribution) was calculated with the same velocity data and represented as a contour plot.

Sedimentation equilibrium data were recorded over 30 h at a rotor temperature of 4 °C at increasing speeds of 16,000 to 24,000 rpm using the long column technique.[44] Protein at a concentration of 7.7 μM (150 –160 μl) was loaded into double-sector centrepieces and absorbance distributions were recorded at 280 and 250 nm in 0.001 cm radial intervals with 10 replicates for each point. Global least squares modelling was performed at multiple wavelengths and rotor speeds with the software SEDPHAT (www.analyticalultracentrifugation.com) using a single-species model.

Molecular Dynamics Simulations

Molecular dynamics simulations were performed with the AMBER 9 molecular modeling suite[45] using 16 processors on an IBM BladeServer Linux cluster. The AMBER force field was utilized as previously described,[20] using the Generalized-Born solvent model with a salt concentration of 0.1 M and a non-bonded interaction cut-off of 22 Å. A starting model of full-length p27 bound to Cdk2/cyclin A was constructed as follows. A molecular model of residues 96–198 of p27 in an extended, random conformation was linked via a peptide bond to residue 95 of p27-KID in the structure of p27-KID/Cdk2/cyclin A (PDB ID: 1JSU) using Insight II software (Accelyrs). The starting structure was energy minimized, equilibrated using MD for 100 ps, and then an MD trajectory was computed for 12.7 ns in the presence of a weak harmonic potential of 0.5 kcal mol^{-1} $Å^{-2}$ on Cdk2 and cyclin A in order to maintain the starting structure. However, an independent MD computation performed without this weak restraint did not show substantial changes in the conformations of cyclin A and Cdk2. The MD trajectory was

analyzed using the ptraj module of AMBER. Analysis of the coordinate RMSD fluctuations for Cdk2 and cyclin A using the ptraj module of AMBER showed that the system was equilibrated within 5 ns. Molecular structures taken at 0.1 ns intervals from 5–12.7 ns were analyzed with regard their conformation and were used to compute hydrodynamic parameters for comparison with AUC and SAXS data. Sedimentation coefficient values for this ensemble of structures were calculated using the program HYDROPRO.[21,22]

Small-angle X-ray scattering

Small-angle X-ray scattering (SAXS) data were collected using the Center for Structural Molecular Biology 4 m SAXS instrument, described previously.[46] Data for samples and backgrounds, consisting of buffer solution, were collected and averaged over a total of 19 and 12 hours, respectively. The total time included shorter consecutive exposures (one hour) to test for time-dependent aggregation indicative of radiation damage; none was found. Data were reduced, scaled into absolute units (1/cm) and azimuthally averaged to the 1D intensity profile $I(q)$ vs. q, where $q = 4\pi\sin(\theta)/\lambda$, according to previously published procedures.[46] 2θ is the scattering angle from the direct beam and λ is the X-ray wavelength (1.542 Å).

Small-angle X-ray scattering analysis and modeling

Data were analyzed according to Guinier[23] and Debye[24] for radius of gyration, R_g, which assume a compact structure and a disordered Gaussian chain conformation, respectively. The structure of the complex is expected to contain both compact ordered regions and disordered regions, so neither model is truly ideal for this particular scattering particle. The two methods should provide comparable estimates of R_g. The data were also analyzed for the pair-distance distribution function *P(r)* and maximum linear dimension, d_{max}, using the program GNOM. 47 *P(r)* and *I(q)* are related through the Fourier transform in Equation 1.

$$P(r) = \frac{1}{2\pi^2}\int_0^\infty dq \cdot (qr) \cdot I(q)\sin(qr) \quad (1)$$

The *P(r)* fitting also provides a secondary measure of R_g, which is the second moment of *P (r)*. Low-resolution *ab initio* models and the consensus envelope model of the p27/Cdk2/cyclin A complex were generated using the program GA_STRUCT.[26] To compare the measured intensity against single, high-resolution structures and the MD-generated ensemble of structures, the program ORNL_SAS[25] was used to calculate the expected small-angle X-ray scattering intensity from the atomic coordinates. The quality of the fit of an intensity profile calculated from a structure was evaluated using the reduced χ^2 parameter.[48] To calculate the scattering from the ensemble of structures generated during MD calculations, intensities were calculated for structures taken from 5–12.7 ns at 0.1 ns intervals. The scattered intensity from the ensemble of MD structures was calculated as a superposition of the individual intensities. [27] The quality of fit of the ensemble intensity profile to the experimental data was also determined using the reduced χ^2 parameter.

Supplementary Material

Refer to Web version on PubMed Central for supplementary material.

Acknowledgements

The authors acknowledge Dr. Peter Schuck (National Institutes of Health, Bethesda, MD, USA) for helpful discussion on the analysis of analytical centrifugation data and Yiming Mo (Oak Ridge National Laboraotry, USA) for assistance in collecting SAXS data. This work was supported by the American Lebanese Syrian Associated Charities (ALSAC), National Cancer Institute (2R01CA082491, RWK), and a Cancer Center (CORE) Support Grant (5P30CA021765, St. Jude Children's Research Hospital). SAXS studies were supported by the Oak Ridge Center for Structural Molecular Biology (KP1102010) of the Office of Biological and Environmental Research of the U. S. Department of Energy,

under contract No. DE-AC05-00OR22725 with Oak Ridge National Laboratory, managed and operated by UT-Batelle, LLC. The submitted manuscript has been authored by a contractor of the U.S. Government under Contract DE-AC05-00OR22725. Accordingly, the U.S. Government retains a nonexclusive royalty-free license to publish or reproduce the published form of this contribution, or allow others to do so, for U.S. Government purposes.

References

1. Hengst L, Dulic V, Slingerland JM, Lees E, Reed SI. A cell cycle-regulated inhibitor of cyclin-dependent kinases. Proc Natl Acad Sci USA 1994;91:5291–5. [PubMed: 8202483]
2. Polyak K, Kato JY, Solomon MJ, Sherr CJ, Massague J, Roberts JM, Koff A. p27kip1, a cyclin-Cdk inhibitor, links transforming growth factor-beta and contact inhibition to cell cycle arrest. Genes Dev 1994;8:9–22. [PubMed: 8288131]
3. Toyoshima H, Hunter T. p27, a novel inhibitor of G1 cyclin-Cdk protein kinase activity, is related to p21. Cell 1994;78:67–74. [PubMed: 8033213]
4. Lacy ER, Filippov I, Lewis WS, Otieno S, Xiao L, Weiss S, Hengst L, Kriwacki RW. p27 binds cyclin-CDK complexes through a sequential mechanism involving binding-induced protein folding. Nat Struct Mol Biol 2004;11:358–364. [PubMed: 15024385]
5. Morgan DO. Principles of CDK regulation. Nature 1995;374:131–134. [PubMed: 7877684]
6. Hengst L, Reed SI. Inhibitors of the Cip/Kip family. Curr Top Microbiol Immunol 1998;227:25–41. [PubMed: 9479824]
7. Sherr CJ, Roberts JM. CDK inhibitors: positive and negative regulators of G1-phase progression. Genes Dev 1999;13:1501–12. [PubMed: 10385618]
8. Hengst L, Reed SI. Translational control of p27Kip1 accumulation during the cell cycle. Science 1996;271:1861–4. [PubMed: 8596954]
9. Pagano M, Tam SW, Theodoras AM, Beer-Romero P, Del Sal G, Chau V, Yew PR, Draetta GF, Rolfe M. Role of the ubiquitin-proteasome pathway in regulating abundance of the cyclin-dependent kinase inhibitor p27. Science 1995;269:682–5. [PubMed: 7624798]
10. Grimmler M, Wang Y, Mund T, Cilensek Z, Keidel EM, Waddell MB, Jakel H, Kullmann M, Kriwacki RW, Hengst L. Cdk-Inhibitory Activity and Stability of p27(Kip1) Are Directly Regulated by Oncogenic Tyrosine Kinases. Cell 2007;128:269–80. [PubMed: 17254966]
11. Bloom J, Pagano M. Deregulated degradation of the cdk inhibitor p27 and malignant transformation. Semin Cancer Biol 2003;13:41–7. [PubMed: 12507555]
12. Bloom J, Pagano M, Ababou M, Dutertre S, Lecluse Y, Onclercq R, Chatton B, Amor-Gueret M, Soslow RA, Carlson DL, Horenstein MG, Osborne MP, Bhalla A, Bamezai R. Deregulated degradation of the cdk inhibitor p27 and malignant transformation ATM-dependent phosphorylation and accumulation of endogenous BLM protein in response to ionizing radiation; A comparison of cell cycle markers in well-differentiated lobular and ductal carcinomas MNNG-transformed Bloom syndrome B-lymphoblastoids for the detection of Hodgkin's lymphoma-associated antigen in 2D Westerns. Semin Cancer Biol 2003;13:41–7. [PubMed: 12507555]
13. Slingerland J, Pagano M. Regulation of the cdk inhibitor p27 and its deregulation in cancer. J Cell Physiol 2000;183:10–7. [PubMed: 10699961]
14. Kamura T, Hara T, Matsumoto M, Ishida N, Okumura F, Hatakeyama S, Yoshida M, Nakayama K, Nakayama KI. Cytoplasmic ubiquitin ligase KPC regulates proteolysis of p27(Kip1) at G1 phase. Nat Cell Biol 2004;6:1229–35. [PubMed: 15531880]
15. Kotoshiba S, Kamura T, Hara T, Ishida N, Nakayama KI. Molecular dissection of the interaction between p27 and Kip1 ubiquitylation-promoting complex, the ubiquitin ligase that regulates proteolysis of p27 in G1 phase. J Biol Chem 2005;280:17694–700. [PubMed: 15746103]
16. Sabile A, Meyer AM, Wirbelauer C, Hess D, Kogel U, Scheffner M, Krek W. Regulation of p27 degradation and S-phase progression by Ro52 RING finger protein. Mol Cell Biol 2006;26:5994–6004. [PubMed: 16880511]
17. Chu I, Sun J, Arnaout A, Kahn H, Hanna W, Narod S, Sun P, Tan CK, Hengst L, Slingerland J. p27 Phosphorylation by Src Regulates Inhibition of Cyclin E-Cdk2. Cell 2007;128:281–294. [PubMed: 17254967]

18. Russo AA, Jeffrey PD, Patten AK, Massague J, Pavletich NP. Crystal structure of the p27Kip1 cyclin-dependent-kinase inhibitor bound to the cyclin A-Cdk2 complex. Nature 1996;382:325–331. [PubMed: 8684460]
19. Bienkiewicz EA, Adkins JN, Lumb KJ. Functional consequences of preorganized helical structure in the intrinsically disordered cell-cycle inhibitor p27(Kip1). Biochemistry 2002;41:752–9. [PubMed: 11790096]
20. Sivakolundu SG, Bashford D, Kriwacki RW. Disordered p27(Kip1) Exhibits Intrinsic Structure Resembling the Cdk2/Cyclin A-bound Conformation. J Mol Biol 2005;353:1118–1128. [PubMed: 16214166]Epub 2005 Sep 20
21. Garcia de la Torre J. Building hydrodynamic bead-shell models for rigid bioparticles of arbitrary shape. Biophys Chem 2001;94:265–74. [PubMed: 11804736]
22. Garcia De La Torre J, Huertas ML, Carrasco B. Calculation of hydrodynamic properties of globular proteins from their atomic-level structure. Biophys J 2000;78:719–30. [PubMed: 10653785]
23. Guinier, A.; Fournet, G. Small-angle scattering of X-rays. John Wiley & Sons; New York, NY, USA: 1955.
24. Debye P. Molecular-weight determination by light scattering. Journal of Physical and Colloid Chemistry 1947;51:18–32.
25. Tjioe E, Heller WT. ORNL_SAS: software for calculation of small-angle scattering intensities of proteins and protein complexes. Journal of Applied Crystallography 2007;40:782–785.
26. Heller WT, Krueger JK, Trewhella J. Further insights into calmodulin-myosin light chain kinase interaction from solution scattering and shape restoration. Biochemistry 2003;42:10579–88. [PubMed: 12962481]
27. Heller WT. Influence of multiple well defined conformations on small-angle scattering of proteins in solution. Acta Crystallogr D Biol Crystallogr 2005;61:33–44. [PubMed: 15608373]
28. Bienkiewicz EA, Adkins JN, Lumb KJ. Functional consequences of preorganized helical structure in the intrinsically disordered cell-cycle inhibitor p27(Kip1). Biochem 2002;41:752–759. [PubMed: 11790096]
29. Hao B, Zheng N, Schulman BA, Wu G, Miller JJ, Pagano M, Pavletich NP. Structural basis of the Cks1-dependent recognition of p27(Kip1) by the SCF(Skp2) ubiquitin ligase. Mol Cell 2005;20:9–19. [PubMed: 16209941]
30. Buck M, Xu W, Rosen MK. A two-state allosteric model for autoinhibition rationalizes WASP signal integration and targeting. J Mol Biol 2004;338:271–85. [PubMed: 15066431]
31. Remenyi A, Good MC, Lim WA. Docking interactions in protein kinase and phosphatase networks. Curr Opin Struct Biol 2006;16:676–85. [PubMed: 17079133]
32. Neduva V, Russell RB. Linear motifs: evolutionary interaction switches. FEBS Lett 2005;579:3342–5. [PubMed: 15943979]
33. Kriwacki RW, Hengst L, Tennant L, Reed SI, Wright PE. Structural studies of p21(waf1/cip1/sdi1) in the free and Cdk2-bound state: Conformational disorder mediates binding diversity. Proc Natl Acad Sci USA 1996;93:11504–11509. [PubMed: 8876165]
34. Grimmler M, Wang Y, Mund T, Cilensek Z, Keidel EM, Waddell MB, Jakel H, Kullmann M, Kriwacki RW, Hengst L. Cdk-inhibitory activity and stability of p27Kip1 are directly regulated by oncogenic tyrosine kinases. Cell 2007;128:269–80. [PubMed: 17254966]
35. Wang Y, Filippov I, Richter C, Luo R, Kriwacki RW. Solution NMR studies of an intrinsically unstructured protein within a dilute, 75 kDa eukaryotic protein assembly; probing the practical limits for efficiently assigning polypeptide backbone resonances. Chembiochem 2005;6:2242–6. [PubMed: 16270364]
36. Neidhardt FC, Bloch PL, Smith DF. Culture medium for enterobacteria. J Bact 1974;119:736–747. [PubMed: 4604283]
37. Grzesiek S, Bax A. Improved 3D triple resonance NMR techniques applied to a 31 kDa protein. J Magn Reson 1992;96:432–440.
38. Grzesiek S, Dobeli H, Gentz R, Garotta G, Labhardt AM, Bax A. 1H, 13C, and 15N NMR backbone assignments and secondary structure of human interferon-gamma. Biochemistry 1992;31:8180–8190. [PubMed: 1525157]

39. Wittekind M, Mueller L. HNCACB, a high-sensitivity 3D NMR experiment to correlate amide-proton and nitrogen resonances with the alpha- and beta-carbon resonances in proteins. J Magn Reson B 1993;101:201–205.
40. Yamazaki T, Lee W, Arrowsmith CH, Muhandiram DR, Kay LE. A suite of triple resonance NMR experiments for the backbone assignment of 15N, 13C, 2H labeled proteins with high sensitivity. J Amer Chem Soc 1994;116:11655–11666.
41. Delaglio F, Grzesiek S, Vuister GW, Zhu G, Pfeifer J, Bax A. NMR Pipe: A multidimensional spectral processing system based on UNIX pipes. J Biomol NMR 1995;6:277–293. [PubMed: 8520220]
42. Cavanagh, J.; Fairbrother, WJ.; Palmer, AG., III; Skelton, NJ. Protein NMR Spectroscopy. Academic Press; New York: 1996.
43. Schwarzinger S, Kroon GJ, Foss TR, Chung J, Wright PE, Dyson HJ. Sequence-dependent correction of random coil NMR chemical shifts. J Am Chem Soc 2001;123:2970–8. [PubMed: 11457007]
44. Vistica J, Dam J, Balbo A, Yikilmaz E, Mariuzza RA, Rouault TA, Schuck P. Sedimentation equilibrium analysis of protein interactions with global implicit mass conservation constraints and systematic noise decomposition. Anal Biochem 2004;326:234–56. [PubMed: 15003564]
45. Case, DA.; Darden, TA.; Cheatham, ITE.; Simmerling, CL.; Wang, J.; Duke, RE.; Luo, R.; Merz, KM.; Pearlman, DA.; Crowley, M.; Walker, RC.; Zhang, W.; Wang, B.; Hayik, S.; Roitberg, A.; Seabra, G.; Wong, KF.; Paesani, F.; Wu, X.; Brozell, S.; Tsui, V.; Gohlke, H.; Yang, L.; Tan, CK.; Mongan, J.; Hornak, V.; Cui, G.; Beroza, P.; Mathews, DH.; Schafmeister, C.; Ross, WS.; Kollman, PA. AMBER 9. University of California; San Francisco: 2006.
46. Woodward JD, Pickel JM, Anovitz LM, Heller WT, Rondinone AJ. Self-assembled colloidal crystals from ZrO2 nanoparticles. J Phys Chem B Condens Matter Mater Surf Interfaces Biophys 2006;110:19456–60. [PubMed: 17004805]
47. Svergun DI. Determination of the regularization parameter in indirect-transform methods using perceptual criteria. J Appl Crystallogr 1992;25:495–503.
48. Taylor, JR. An Introduction to Error Analysis: The Study of Uncertainties in Physical Measurements. 2. University Science Books; Sausalito, CA, USA: 1997.
49. Koradi R, Billeter M, Wuthrich K. MOLMOL: a program for display and analysis of macromolecular structures. J Mol Graph 1996;14:51–5. 29–32. [PubMed: 8744573]
50. Kozin MB, Svergun DI. Automated matching of high- and low-resolution structural models. Journal of Applied Crystallography 2001;34:33–41.

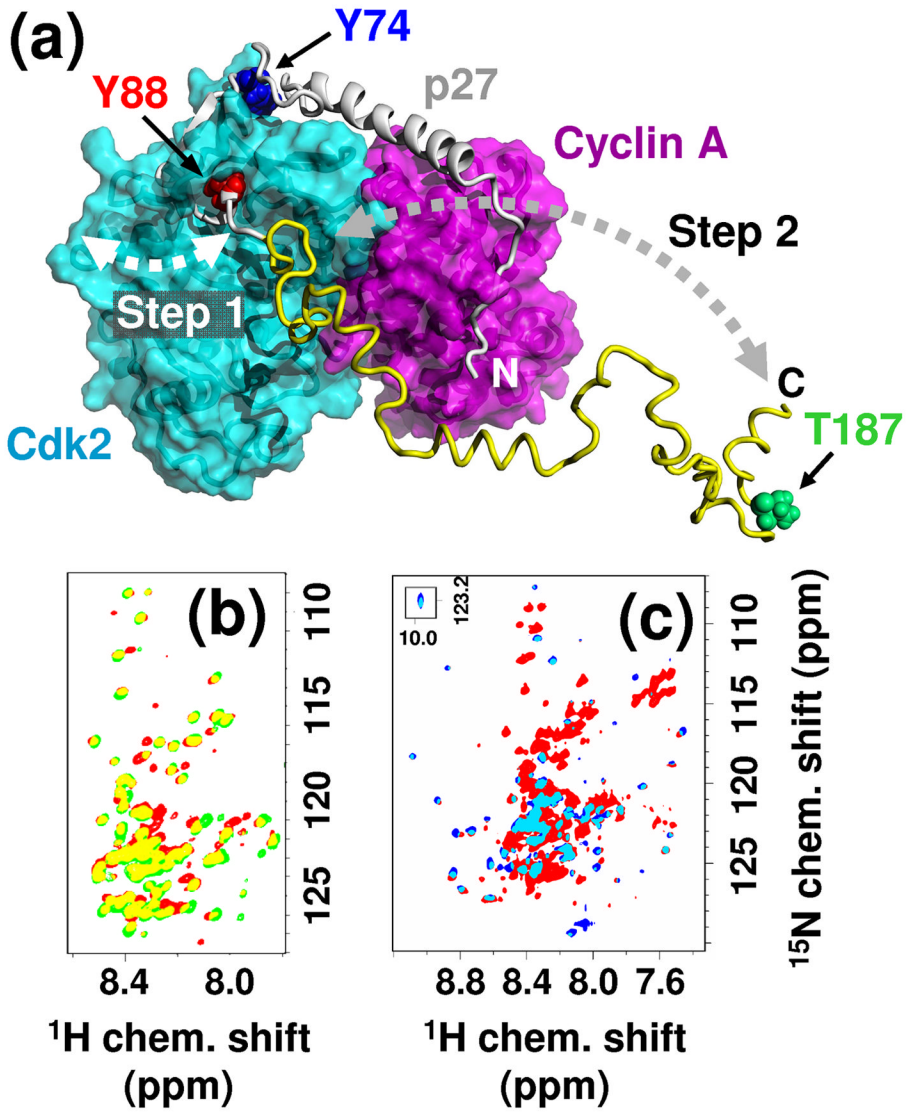

Figure 1.

Structure of the p27/Cdk2/cyclin A complex. (a) Schematic view prepared with the program PyMOL (http://pymol.sourceforge.net) of full-length p27 bound to Cdk2/cyclin A showing the solvent accessible surface for Cdk2 (cyan) and cyclin A (magenta). The kinase inhibitory domain (KID) (grey) and C-terminal domain (yellow) of p27 are illustrated as ribbons. The structure shown was obtained at 7.3 ns during the MD trajectory. (b) 2D ^{1}H-^{15}N HSQC spectrum of p27-C (green) overlaid with the 2D ^{1}H-^{15}N TROSY spectrum of $^{2}H/^{15}N$-p27 bound to unlabeled Cdk2/cyclin A (red) where overlapping resonances are colored yellow. (c) 2D ^{1}H-^{15}N HSQC spectrum of p27-KID (blue) overlaid with the 2D ^{1}H-^{15}N TROSY spectrum of $^{2}H/^{15}N$- p27 bound to unlabeled Cdk2/cyclin A (red) where overlapping resonances are colored cyan.

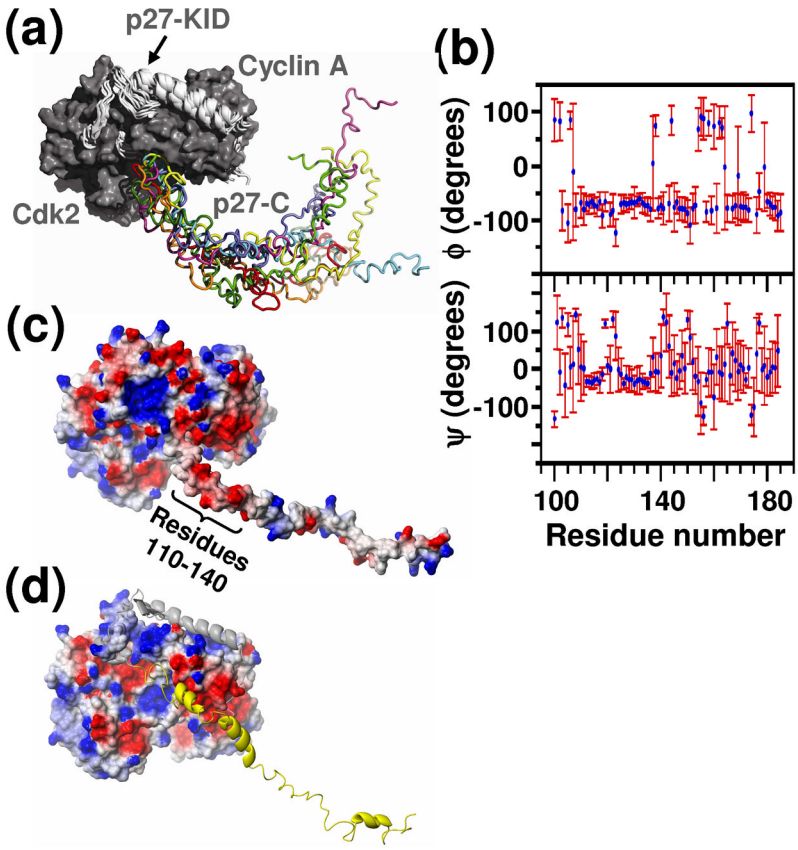

Figure 2.

Conformational flexibility of the C-terminal domain of p27 in the p27/Cdk2/cyclin A complex. Superposition of p27/Cdk2/cyclin A structures at varying time intervals during a 12.7 ns molecular dynamics simulation (5 ns – magenta, 6.1 ns – yellow, 7.2 ns – light green, 8.3 ns – cyan, 9.4 – blue, 10.5 ns – orange, 11.6 ns – red, 12.7 ns – dark green). The solvent accessible surface for Cdk2/cyclin A is colored grey. The figure was generated using the program PyMol. (b) Summary of average Ψ and φ torsion angle values for residues in the C-terminal domain of p27 over the course of the MD simulation. Error bars indicate RMSD values for Ψ and φ torsion angles during the simulation. (c) and (d) Electrostatic repulsion between the C-terminal region of p27 and the surface of the Cdk2/cyclin A complex. Electrostatic potential surface generated with the program MOLMOL[49] for the (c) p27/Cdk2/cyclin A complex and (d) Cdk2/cyclin A complex where p27 is illustrated as a ribbon and is colored according to Figure 1. The structure shown was obtained at 8.3 ns during the MD trajectory.

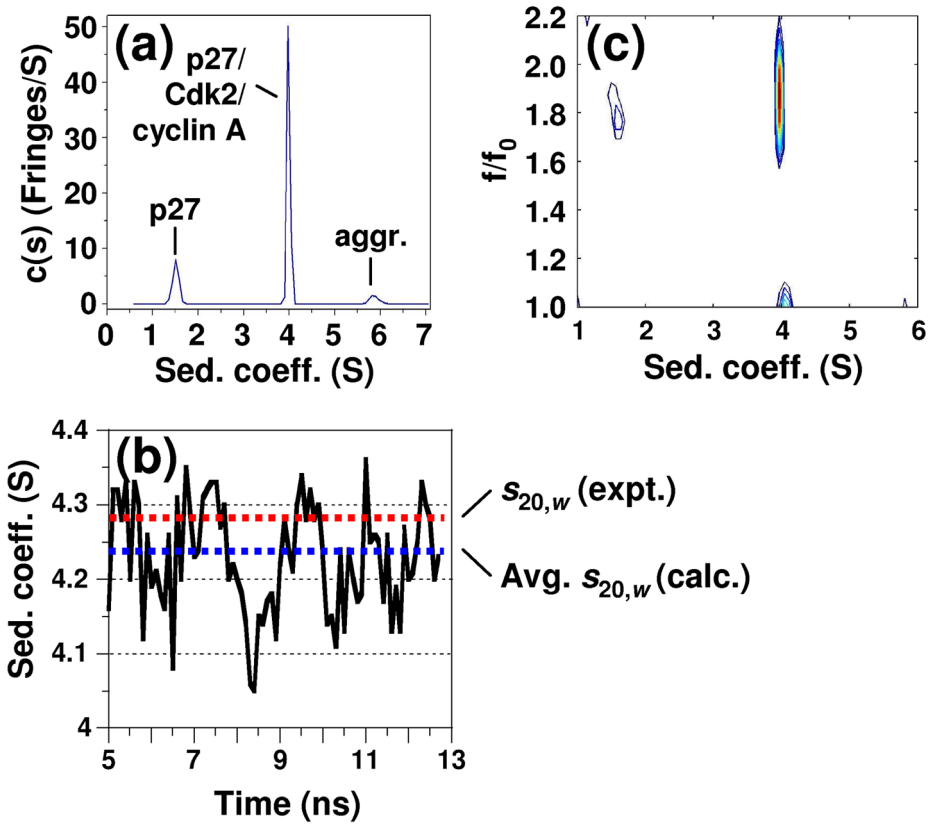

Figure 3.

Hydrodynamic studies of the p27/Cdk2/cyclin A ternary complex. (a) Interference fringe displaced velocity data for p27/Cdk2/cyclin A were analyzed using the continuous sedimentation coefficient distribution, *c (s)*, model with the *c (s)* distributions displayed in fringes/S *versus* sedimentation coefficient (*s*). Experiments were conducted at 20 °C at a rotor speed of 50,000 rpm and a starting protein concentration of 2 mg/ml (24 μM). The *s*-value of the complex was determined as 3.98 S with a best-fit weight-average frictional ratio $(f/f_0)_w$ of 1.63 and a calculated molecular mass of 87,603 Da. This analysis was with regularization at a confidence level of p = 0.7 and at a resolution of sedimentation coefficients of n = 100. The peak at ~1.5 S marked “p27” corresponds to a small amount of unbound p27 and that marked “aggr.” corresponds to a small amount of unidentified protein aggregate. (b) Calculated sedimentation coefficients computed using the program HYDROPRO for p27/Cdk2/cyclin A structures from the MD trajectory. The red dotted line represents the standard value based the experimental *s*-value and the blue dotted line represents the average of the calculated *s*-values. (c) Contour plot of the two-dimensional *c* (*s*, f/f_0) distribution calculated using SEDFIT with an equidistant f/f_0 -grid from 1.0 to 2.2 with 0.1 steps, a linear *s*-grid from 1 to 8 S, a resolution of 100 s-values and regularization at one standard deviation. The differently colored contours represent *c* (*s*, f/f_0)-values from 0 fringes/S (white) to 1.0 fringes/S (red), with increasing color temperature indicating larger values.

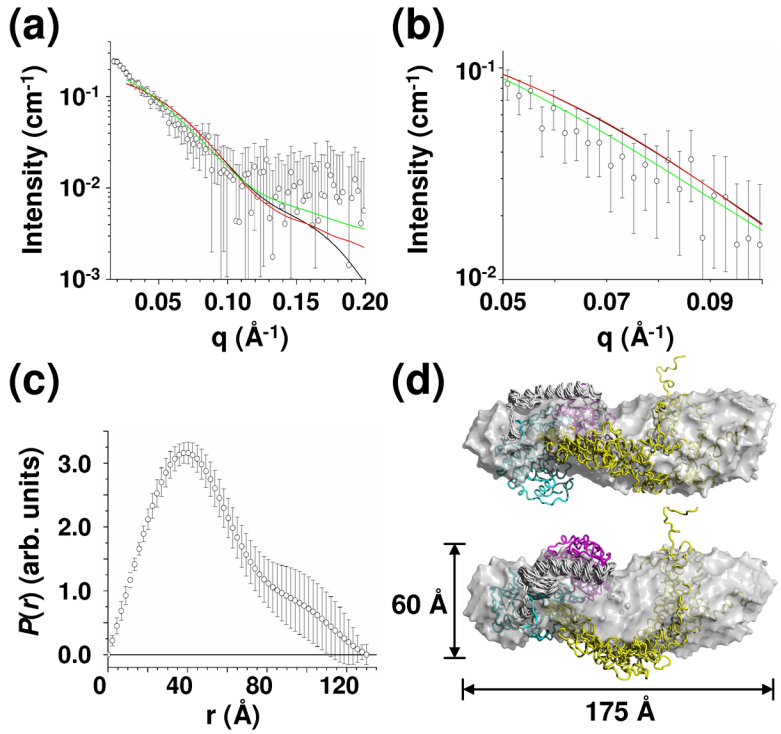

Figure 4.

The p27/Cdk2/cyclin A complex adopts an extended conformation in solution. (a) SAXS data for the p27/Cdk2/Cyclin A complex (○). Profiles calculated with the program ORNL_SAS using p27-KID/Cdk2/cyclin A (PDB 1JSU) (black), p27/Cdk2/cyclin A in which p27 was fully extended ($p27^{EX}$) (red), and the MD-generated ensemble of p27/Cdk2/cyclin A structures (green). (b) Expanded view of the SAXS data region used for quantitative comparison with calculated data. (c) *P*(*r*) derived from the SAXS data using the program GNOM.[47] (d) Two orthogonal views of a surface representation of the consensus envelope generated by GA_STRUCT[26] from SAXS data of the p27/Cdk2/Cyclin A complex. The best-fit of representative MD-generated structures of p27/Cdk2/cyclin A (shown as tubes) to the envelope determined by SUPCOMB[50] is illustrated in the figure. The color scheme is the same as used in Fig. 1a and the figure was generated using PyMOL.

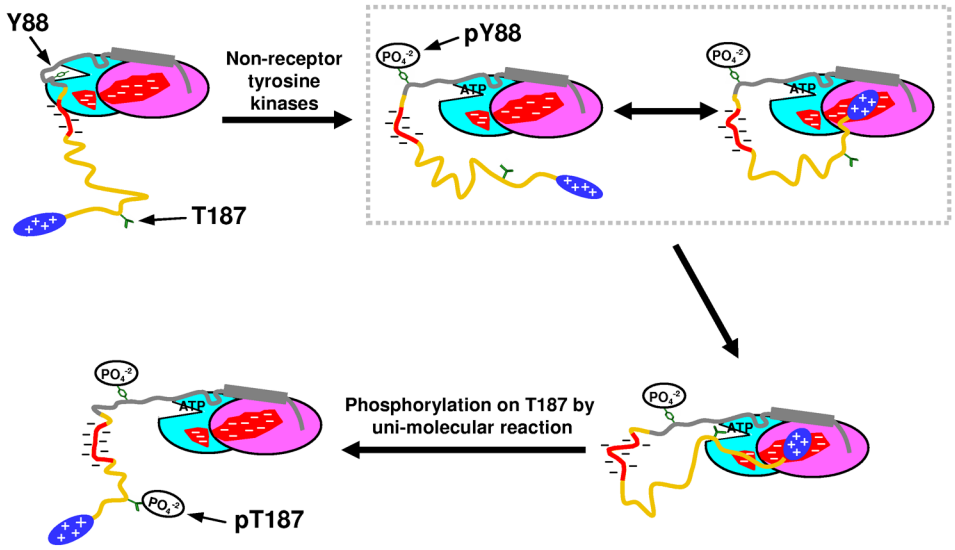

Figure 5.

Schematic highlighting the importance of p27 flexibility in transducing NRTK signals which mediate p27 degradation and cell cycle progression. The p27/Cdk2/cyclin A complex is colored according to Fig. 1a. Regions of positive and negate electrostatic potential are colored blue and red, respectively. Phosphorylation of Y88 within the 3_{10} helix of the kinase inhibitory domain of p27 by various NRTKs leads to its ejection from the ATP binding pocket of Cdk2 and partial re-activation of Cdk2. This may be facilitated by electrostatic repulsion between negatively charged residues on the surface of Cdk2/cyclin A and residues of p27. In addition, binding of the C-terminal region of p27 adjacent to T187 to the surface of Cdk2/cyclin A may be enhanced by electrostatic attraction between negatively and positively charged residues on Cdk2/cyclin A and p27, respectively. This binding would enhance the Cdk2-mediated phosphorylation of T187. Once phosphorylated, T187, which lies within the flexible C-terminal region of p27, is fully exposed and recognized by SCF/Skp2 which poly-ubiquitinates p27.